CLARIFICATION OF UNSTEADY CHARACTERISTICS IN SEPARATED FLOW OVER AN AXISYMMETRIC PARABOLOID AT HIGH ANGLES OF ATTACK

Tadateru Ishide [1], Nobuhide Nishikawa [2] and Fumihiko Mikami [2]
1)Kisarazu National College of Technology , 2-11-1,kiyomidai-higashi , Kisarazu City
2)Chiba University , 1-33 , yayoi-cho , inage-ku , Chiba City

Abstract

The phenomenon of three-dimensional separation of the flow over a slender body at high angles of attack is difficult to model and still challenging problem. The singularity of the flow is caused by mutual intervention of three-dimensional separation and separated vortices. In this study, the flow in the cross-flow separation region of an axisymmetric paraboloid at 40 and 50 deg angle of attack has been investigated experimentally by hot wire anemometer. Reynolds numbers are 9.0×10^3 and 1.8×10^4 referred to the base diameter. X-type probe was used to measure three dimensional velocity fluctuations over the axisymmetric paraboloid at sampling time of 4kHz. It has been shown that the lift-off and mergence of vortices can be explained by r.m.s. distribution of velocity fluctuations. Reynolds stress and the difference between probability density function and normal distribution fluctuate where the kink of vortex is observed.

1 Introduction

The flow around a slender body at high angle of attack has been often seen in the field of aerospace, and has been studied from both experiment and numerical analysis. In particular, the data not only in high free stream velocity but also in low free stream velocity have been required in withdrawing and landing of space vehicle. The property in low free stream velocity is nearly complicated as in high free stream velocity, and have been varied in terms of many parameters, such as angle of attack, Reynolds number, apex angle of axisymmetric body and so on. Furthermore, the flow patterns of separated region and wake over a body at high angles of attack have become extremely complicated[1], it has been predicted that those flow patterns cause nonlinearity and singularity of aerodynamic force acting on a body. Therefore, it is of considerable practical significance to understand the properties of the flow qualitatively and quantitatively. From such point of view, the effect of a boundary layer flow for the separated region[2,3], and a geometric definition of the three dimensional separation points , and a quantitative definition of that by measurement of Reynolds stress and wall shear stress have been proposed by several researchers specialized in an axisymmetric body[4,5,6,7]. Various studies have been carried out because at high angles of attack, separated vortices becomes asymmetric, and these asymmetric vortices give rise to significant side forces and yawing moments[8,9,10,11]. Additionally, the recent development of visualization technique have enabled the investigation of cross sectional structure of separated vortices in detail[1,11]. In recent years, for an axisymmetric paraboloid, the authors have reported the measurement of the boundary layer thickness, and assessing the power spectrum of velocity data using a hot wire anemometer which has a I-type probe[12]. Furthermore, the positional variations of both the separation line and the separated vortices in the overall axisymmetric paraboloid have been

shown by a flow visualization technique which consists of the tracer method and laser light sheet method, as well as an image processing, after that the quantitative classification of the separation lines has been performed by considering the maximum value of the power spectrum[13]. In the recent authors' study[14)15], the three dimensional velocity distribution in the separated vortices formed over axisymmetric paraboloid has been measured in detail using hot wire anemometer having a X-type probe , as a result , it has been demonstrated that the r.m.s. value of velocity fluctuation has a maximum in the region of secondary vortex near the body surface at each angle of attack. No definitive work exists, however, on the unsteady characteristics over the whole separated vortex region : the turbulent effect of the mergence of separated vortices , the lift-off of those vortices and the kink of those vortex cores documented by Kubota et al. for the flow in the separated vortices. In the present study, the velocity distribution in the separated flow region over an axisymmetric paraboloid has been measured in detail using a hot wire anemometer having a X-type probe, and the distribution of both r.m.s. value of velocity fluctuation and Reynolds stress have been calculated , the classification of the separated vortices has been carried out using probability density function. Thus, the objective of the present work is to describe quantitatively the vortex mergence, the vortex lift-off and the kink of vortex core.

2 Experimental setup

 The wind tunnel used in this study is the Goettingen type. The test section is 400$\times$ 400 mm, and length of the section is 650mm. The model was made of stainless steel. This model is an axisymmetric paraboloid, whose radius r is represented by $r=\sqrt{x}$ with x, the axial distance from the vertex of the model. The nose length L of the model is 140mm, and at the position of $x=L$ diameter D is 75mm. The model is coaxially connected to a 300mm length cylinder as shown in Fig.1.

3 Experimental approach

The hot wire anemometer in this experiment is the type of constant temperature .The average and the fluctuation of the velocity fields around the body have been measured by this apparatus. This measurement system consists of two constant temperature velocimetry units and a unit measuring temperature for temperature compensation. As measurement in the cross-section of the body, measuring points in the circumferential direction are nine with equal spacing 11.25$°$ at 90$°$ $<\theta<$180$°$. Further two points near secondary vortex, which is confirmed by visualization picture[13] are added for measuring points. In z-direction measuring points are 20 from the origin which is 0.5mm above the body surface to external flow region. As measurement near the body surface, the points above 1.0mm the body surface over the whole of the body are the measuring points. X-type probe was used, and velocity vectors and velocity fluctuation are calculated. The procedure for measuring was as follows. We use two probes and measure the velocity field over the axisymmetric body by changing the probe arrangement: first the tungsten-wire in the vertex of the probe is placed in x-y plane (UV probe), after that by rotating UV probe for 90 degree tungsten-wire is placed in x-z plane (UW probe). Three dimensional velocity components are evaluated in these procedures. The calibration method was shown as follows. After the hot wire probe and a pitot tube were set in the test section, the calibration curve of quaternary order was obtained by relating the
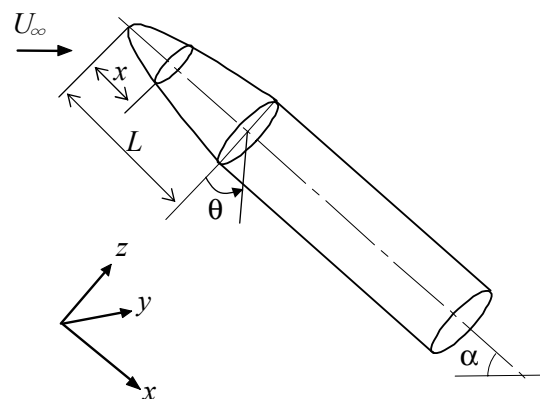
Fig.1 Model and coordinate system

output volts of the hot wire and the velocity assessed using the pitot tube, varying the uniform velocity every 1m/s from 0m/sec to 10m/sec. In this experiment sampling frequency is 4kHz, and data number is 16,384.

4 Results and Discussion

In this experiment, angles of incidence was set at 40 and 50 deg. Main flow velocities are 1.8m/s and 3.6m/s: Reynolds numbers are 9.0×10^3 and 1.8×10^4 respectively reffered to 75mm base-diameter at $x=L$=140mm. The quantitative properties of the longitudinal vortices have been investigated. The residual turbulence of wind tunnel in this experiment is 0.7% in the case of U_∞=1.8m/sec, and 1.1% in the case of U_∞=3.6m/sec. The uniformity of velocity profile at the test section of the wind tunnel is 0.8% in the case of U_∞=1.8m/sec, and 2.6% in the case of U_∞=3.6m/sec. Fig.2 shows visualization picture at 40° of incidence angle, Re=9.0×10^3, x/L=1.0. This picture is obtained by the present authors' visualization experiments[13]. Main, primary, secondary and tertiary vortices are formed in the region from symmetry line of leeward side to circumferential windward side. The direction of rotation of the adjacent vortices is reversal each other. The longitudinal vortices are generated interactively after main vortex has formed by the separated flow originated with the primary separation line and the reattachment flow from the symmetry line of leeward side.

4.1 R.M.S. distribution of velocity fluctuation

Fig.3 shows r.m.s. distribution of v : the velocity component of y-direction at α=40° , Re=9.0×10^3. The r.m.s. value is normalized with respect to the uniform velocity U_∞. The tendency of u and w is the same as v. In this figure , the r.m.s. value shows a maximum in the region of secondary vortex in all cross sections. The values in the region from the primary vortex to the main vortex core, are slightly lower than the values in the secondary vortex. Noting the region where the contour
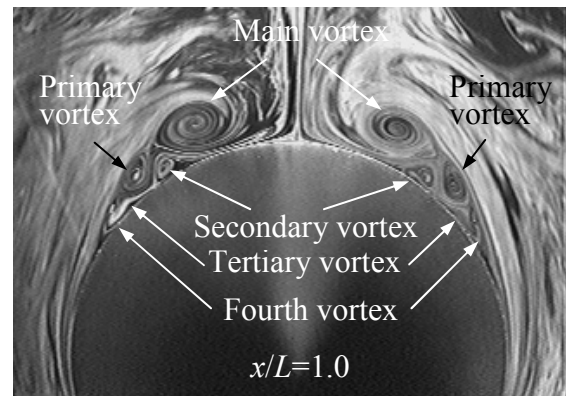
Fig.2 Visualization picture using fog machine
(α=40° ,Re=9.0×10^3)

lines are dense, it is identified that the separated vortex region in the backward of the body becomes extensive. Fig.4 shows r.m.s. distribution at α=40° , Re=1.8×10^4. The point which has a maximum of r.m.s. value, moves to the main vortex region , it is shown that the turbulence generating in the secondary vortex region becomes extended toward main vortex region. Additionally, the point which has a maximum of r.m.s. value exists above the body surface , the lift-off of secondary vortex is confirmed. At x/L=1.0, the point which has a maximum of r.m.s. value exists near the main vortex core lifting off the body surface. The fact indicates the secondary vortex which starts to lift off the body surface at x/L=0.86, is absorbed to the main vortex at x/L=1.0. Further, the region which shows high r.m.s. values exists almost at θ=135° , it is considered that a new secondary vortex has generated. Fig.5 shows r.m.s. distribution at α=50° , Re=1.8×10^4. In this figure , the higher r.m.s. value exists not in the secondary vortex region but in the main vortex region in all cross sections different from α=40° , especially , it is found that the r.m.s. value has a maximum near the main vortex core. As increasing x/L, the main vortex core lifts off the body surface, and the region showing of the high r.m.s. values becomes extensive. Fig.6 shows r.m.s. distribution near body surface at α=40° , Re=9.0×10^3 , 0.21< x/L <1.0. In this figure, it is identified that the r.m.s.
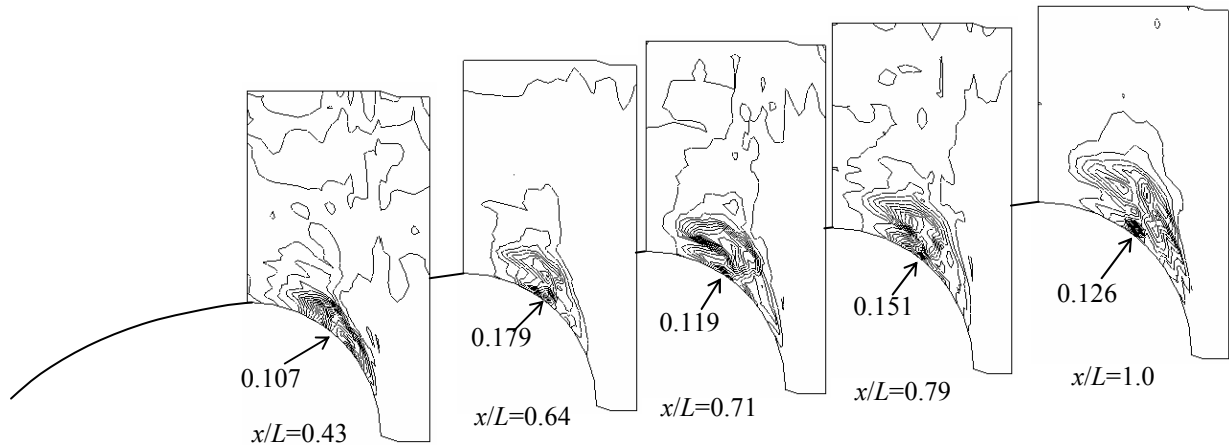
Fig.3 R.M.S. distribution in each cross section (α =40° ,Re=9.0$\times$10^3)
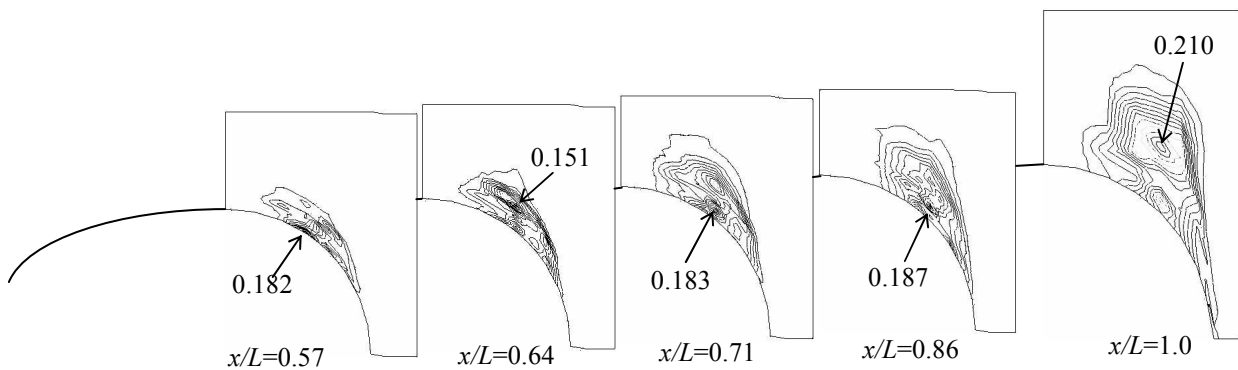
Fig.4 R.M.S. distribution in each cross section (α =40° ,Re=1.8$\times$10^4)
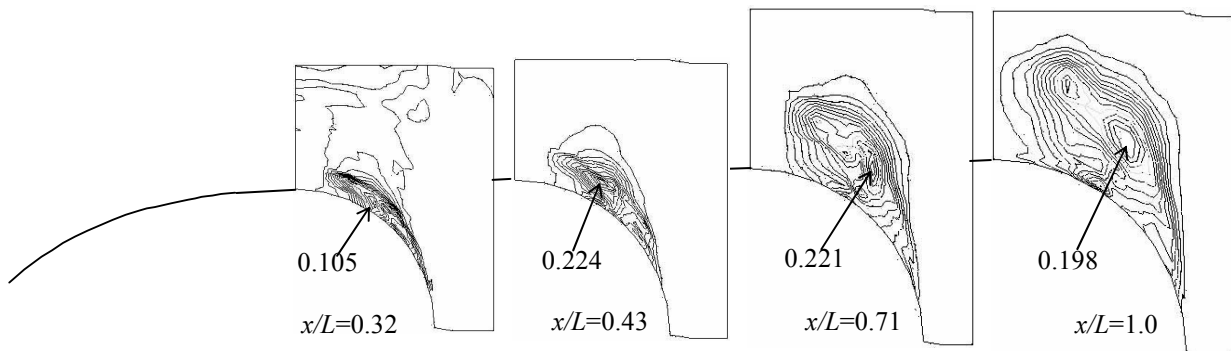
Fig.5 R.M.S. distribution in each cross section (α =50° ,Re=1.8$\times$10^4)

values in the secondary vortex near θ =146° , are extremely high over the whole of the body.

4.2 Classification of separated vortices using probability density function

The r.m.s. value above mentioned can be calculated largely , if the amplitude of velocity fluctuation is large and the fluctuation frequency is low. Thus in this study, the classification of the flow in the separated vortices near body surface has been attempted using probability density function. The probability density function R_1 is calculated from 16,384 sets of sampling data in each measuring point , and the normal distribution R_2 is derived from the standard deviation σ . We introduce the following evaluation function Dfn .

$$Dfn = \int_{v_1}^{v_2}(R_1 - R_2)^2\, dv \qquad (1)$$

v_1 is the minimum value , and v_2 is the maximum value of the sampling data. Fig.7 shows the distribution configuration of the probability density function at $\alpha=40°$, $Re= 9.0\times10^3$. There are large differences between the two distribution configurations at $x/L= 0.86$, $\theta=135°$ and $x/L= 0.79$, $\theta=141°$ .If the r.m.s. values are nearly equal , the probability density function is the almost same as normal distribution in the case of turbulent flow where the amplitude of velocity fluctuation is large , and the frequency of fluctuation is high such as measuring point at $x/L= 0.86$, $\theta=135°$. While , it is considered that the lower frequency components exist in the distribution configuration of measuring point at $x/L= 0.79$, $\theta=141°$. Fig.8 shows the contour of $(1/Dfn)$ at $0.21< x/L<1.0$. In this figure, the distribution configuration of the probability density function is inconsistent with the r.m.s. value , therefore it is confirmed that the regions having normal distribution exist in several places. In this study, we note the value multiplied r.m.s. value by Dfn value. Consequently, the regions , where the low frequency components exist and where the r.m.s. values are high , are detected. Fig.9 shows the contour of the product $(rms\times Dfn)$ near the body surface at $\alpha=40°$, $Re= 9.0\times10^3$. In this figure , the product $(rms\times Dfn)$ values are high along the secondary vortex region , especially the values at $0.64< x/L<0.79$ show a maximum. In this region, the phenomenon of the switching flows, which are low frequency and differs in the mean velocity and the amplitude of velocity fluctuation, could have occurred. In the present authors' visualization experiments[14)15)], the phenomenon of the kink of secondary vortex core is identified as shown with circles in Fig.10(a). The distribution of the product $(rms \times Dfn)$ in Fig.9 shows this phenomenon quantitatively. Fig.11 shows the contour of the product $(rms \times Dfn)$ near the body surface at $\alpha=40°$, $Re= 1.8\times10^4$. In this figure , it is found that the region in $0.43<$
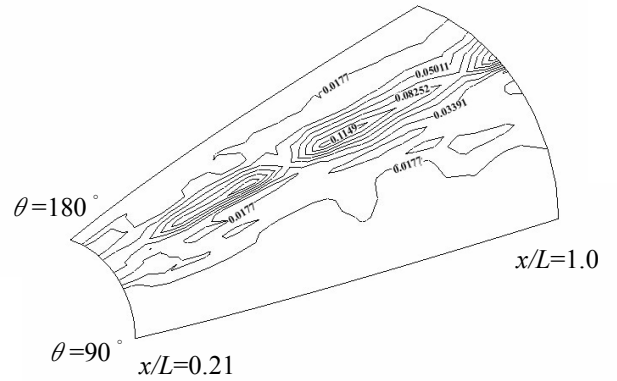
Fig.6 R.M.S. distribution near body surface ($\alpha=40°$,$Re=9.0\times10^3$)
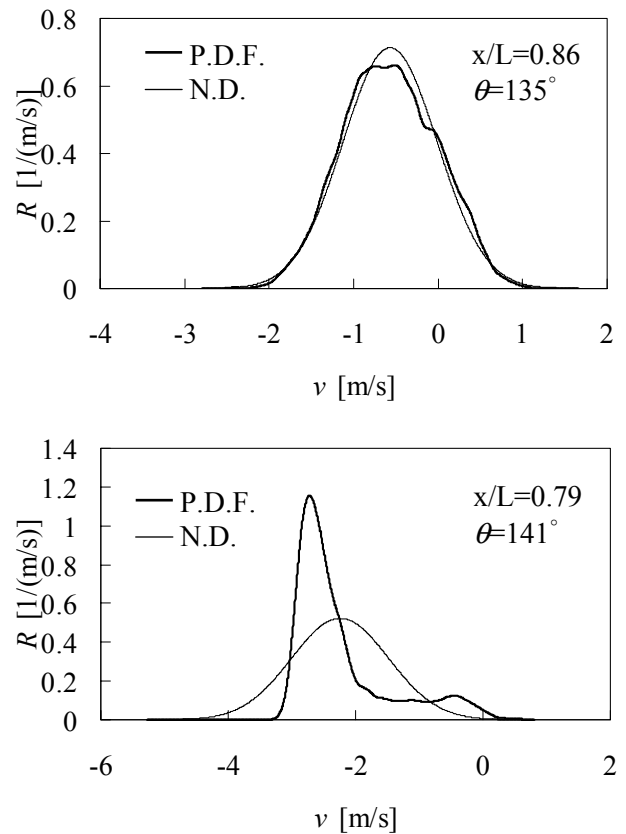
Fig.7 Distribution configuration of the probability density function ($\alpha=40°$,$Re=9.0\times10^3$)

$x/L<1.0$, $145° < \theta<157.5°$ shows high values of the product $(rms\times Dfn)$. In Fig.10(b) , this high value region coincides with the region where the position of the secondary vortex core fluctuates as shown with circles in this figure. Additionally , the profile of the probability density function has two vertexes near $x/L=0.64$, $\theta=140°$. Fig.12 shows the contour of the product $(rms\times Dfn)$ near the body surface at α

=50° , Re= 9.0×10^3. The region A in 0.21< x/L <1.0 , 90° < θ <101° , The region B in 0.64< x/L <1.0 , 101° < θ <129° and the region C in 0.36< x/L <0.57 , 135° < θ <168° have the higher values. Therefore , the regions showing high values exist in several places different from that at α =40° . Since this finding leads to the tendency of the discontinuity of the shear layer proposed by Kubota et al[1]. about the mechanism of the growth of three dimensional separated vortices, it is considered to the reason which cause an asymmetric separated vortices. Fig.13 shows the contour of the product ($rms \times Dfn$) in each cross section at α =40° , Re= 9.0×10^3. The primary and secondary vortex regions at 0.64< x/L <0.79 have higher values of the product ($rms \times Dfn$). The distribution profiles of probability density function in these regions are considerably different from normal distribution the components of low frequency are included
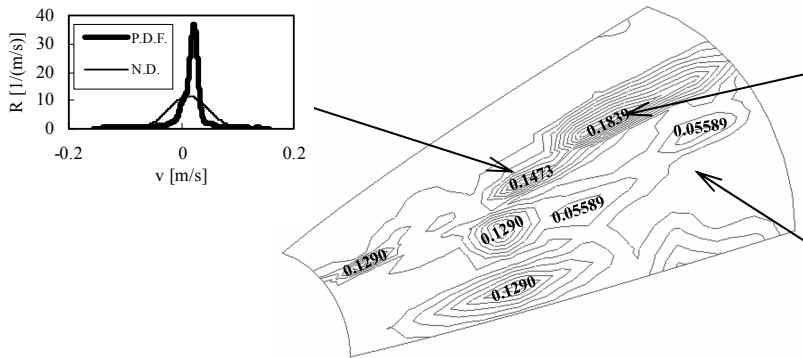
in the measuring data in those regions. The region showing the high value becomes extensive at x/L=1.0, and the center of the contour lifts off the body surface. This finding indicates the phenomenon of lifting off primary and secondary vortices. Fig.14 shows the contour of the product ($rms \times Dfn$) in each cross section at α =40° , Re= 1.8×10^4. The product ($rms \times Dfn$) values are high in the
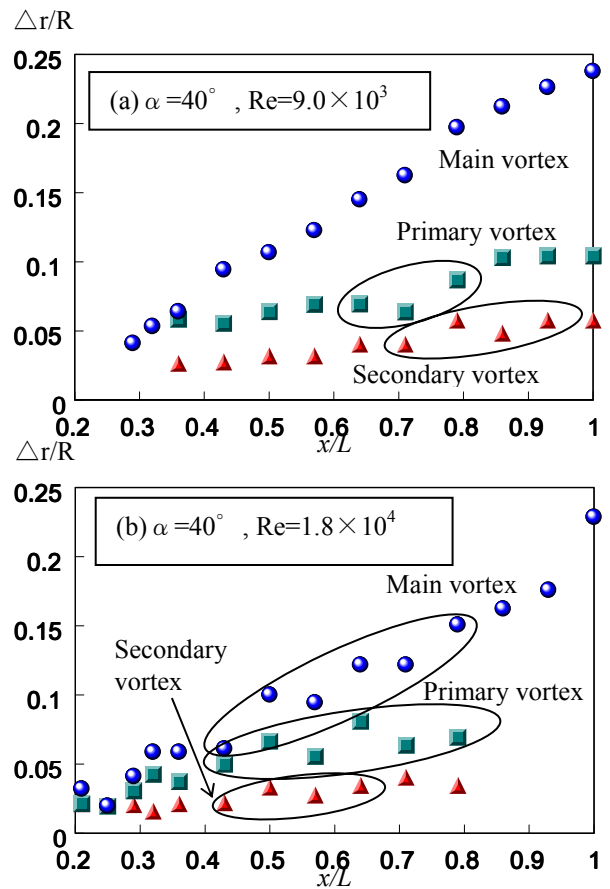
Fig.10 Lift-off of vortex cores in longitudinal vortices

Fig.8 Contour of (1/Dfn) (α =40° , Re=9.0×10^3)

Fig.9 Contour of the product (rms$\times Dfn$) near the body surface (α =40° , Re=9.0×10^3)

primary vortex region at x/L=0.57 , it is validated that the region lifts off the body surface with increasing x/L. Additionally , the product ($rms \times Dfn$) values near the primary separation line at θ =90 ° are large. The maximum value is nearly equal to 0.022 at x/L=0.86, the profile of the probability density function is similar to the normal distribution. It is considered that the flow in this region becomes turbulent. Fig.15 shows the contour of the product ($rms \times Dfn$) in each cross section at α =50° , Re= 1.8×10^4. In this figure , the area from the primary vortex to the main vortex core shows large product ($rms \times Dfn$) value , it is found that the primary vortex is absorbed to the main vortex , and lifts off the body surface with increasing x/L. In the cross sections behind x/L=0.43 , the maximum value of the product ($rms \times Dfn$) is equal to 0.034 , it can be stated that the flow in this regions

becomes turbulent. At x/L=1.0 , the region where the product ($rms \times Dfn$) values are high exists , there are the sweep flow from the main vortex region. The relation between the separated vortex properties and angle of attack α , Reynolds number Re is shown in Table.1 and Fig.16. Table.1 shows the maximum values of the quantity of lifting off the body surface in each separated vortex shown in Fig.10. Fig.16 shows the behavior of the product ($rms \times Dfn$) maximum value. In these table and figure , both of these parameters increase with an increase in α , on the contrary decrease with an increase in Re. Fig.17 shows the contour of Reynolds stress ($u'v'$) in each cross section at α =40° , Re= 9.0×10^3. In this figure, the secondary vortex region near body surface with respect to the main vortex core has a minus value of Reynolds stress, while the region from the primary vortex to the main vortex near the
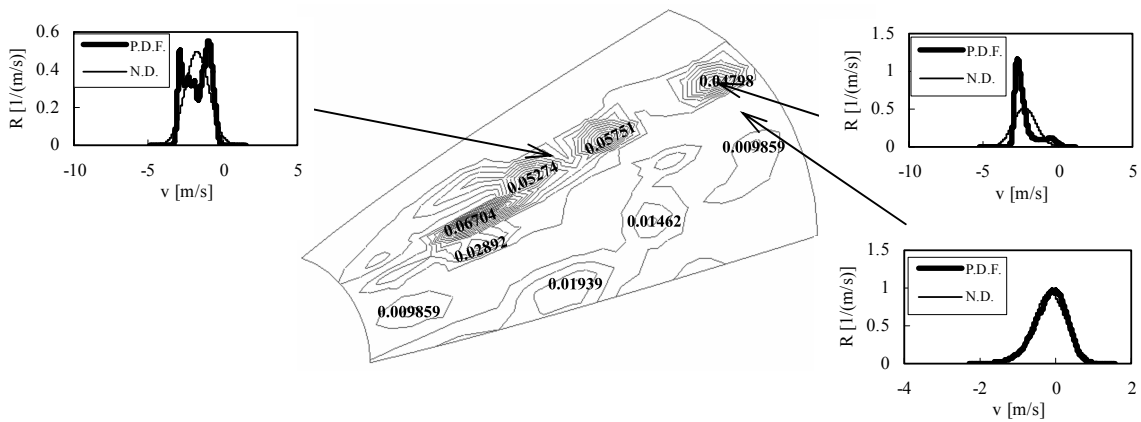
Fig.11 Contour of the product ($rms \times Dfn$) near the body surface (α =40° , Re=1.8×10^4)
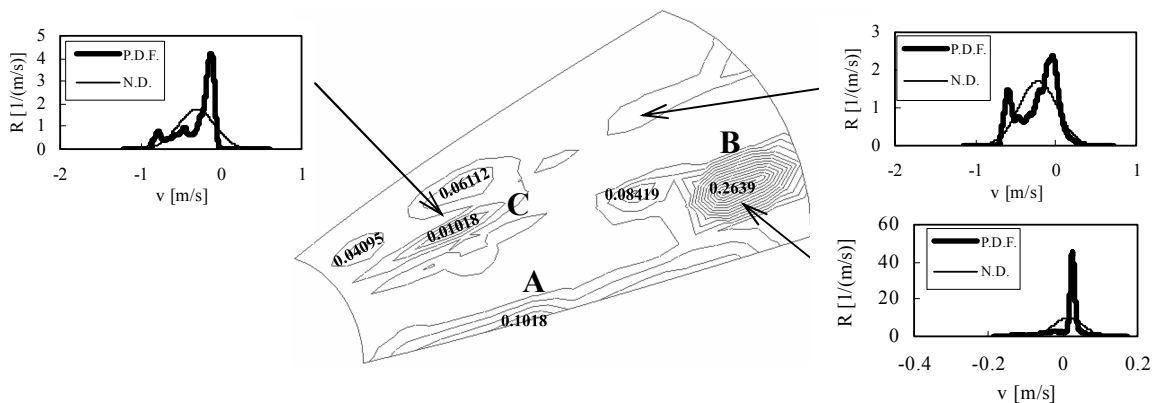
Fig.12 Contour of the product ($rms \times Dfn$) near the body surface (α =50° , Re=9.0×10^3)

external flow with respect to the main vortex core has a plus value of Reynolds stress. Noting the region at 0.64< *x/L* <0.79 including the phenomenon of the kink of the vortex core above mentioned, both the maximum value and the minimum value of Reynolds stress fluctuate. This tendency is observed considerably in the secondary vortex region. At *x/L* =0.71 where the absolute values of Reynolds stress are small , the corresponding product (*rms*×*Dfn*) values are large in Fig.13 : this finding leads to the phenomenon of the switching flow which are low frequency. Fig.18 shows the contour of Reynolds stress (*u'v'*) in each cross section at α=40° , *Re*= 1.8×10^4. The turbulence of the secondary vortex region at *x/L*=0.57 becomes lifted off the main vortex region at *x/L*=0.64. At *x/L*=0.71 , the Reynolds stress near the body surface at θ =140° , *z/R*=0.027(*R*: base-radius at *x/L*=1.0) are large. From these results, it can be stated that the secondary vortex approaches and lifts off the

body surface at 0.57< *x/L* <0.71: this finding is in good agreement with the measurement data of the secondary vortex core positions by visualization experiments in Fig.10(b). It is confirmed that the region where the values of Reynolds stress are large becomes extensive behind *x/L*=0.86, hence the primary vortex is absorbed to the main vortex. Moreover, the maximum value of Reynolds stress increases with increasing *x/L*. Fig.19 shows the contour of Reynolds stress (*u'v'*) in each cross section at α=50° , *Re*= 1.8×10^4. In this figure, the distribution is consistent with the r.m.s. distribution in Fig.5. Therefore, the turbulent separated vortex region becomes extensive behind *x/L*=0.43. And then, the profile of Reynolds stress is extremely complicate as increasing *x/L*, so that the main vortex core fluctuates absorbing the primary vortex, and asymmetrical separated vortices are induced. Fig.20 shows visualization pictures of the separated vortices using Argon-ion laser light
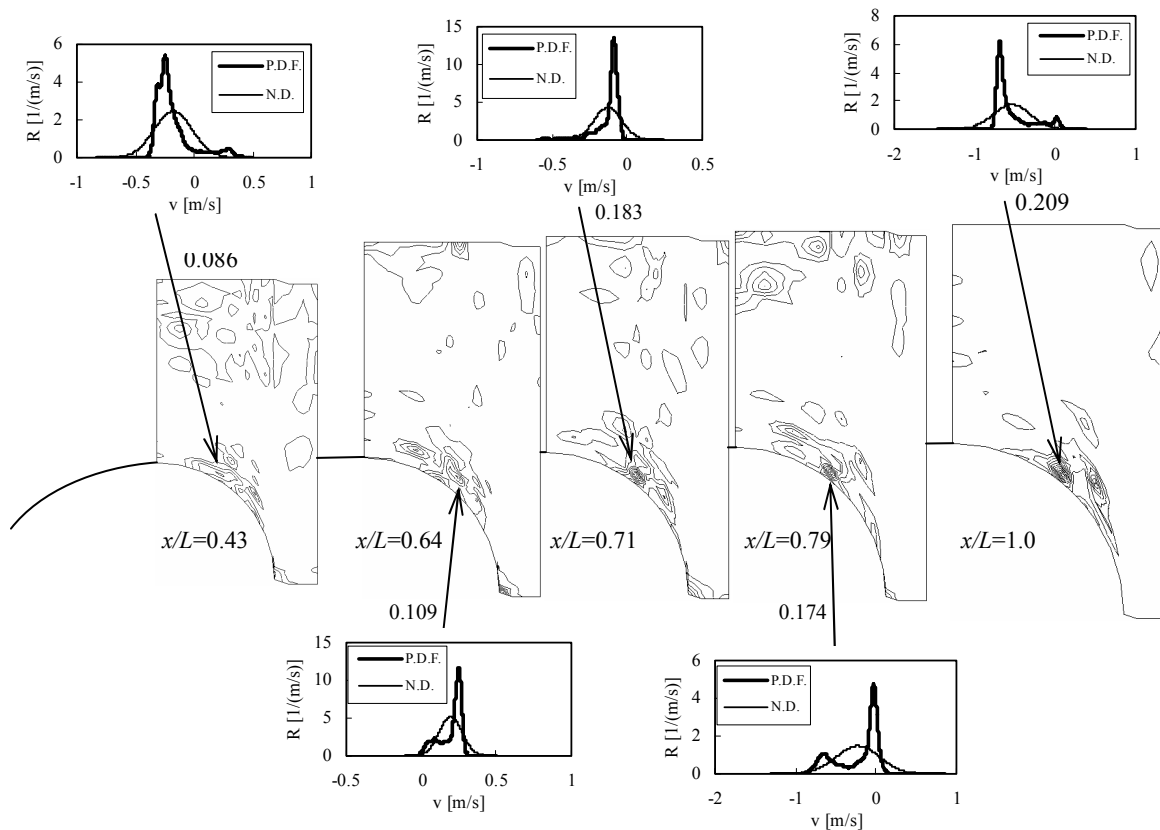
Fig.13 Contour of the product (rms×*Dfn*) in each cross section (α=40° , *Re*=9.0×10^3)
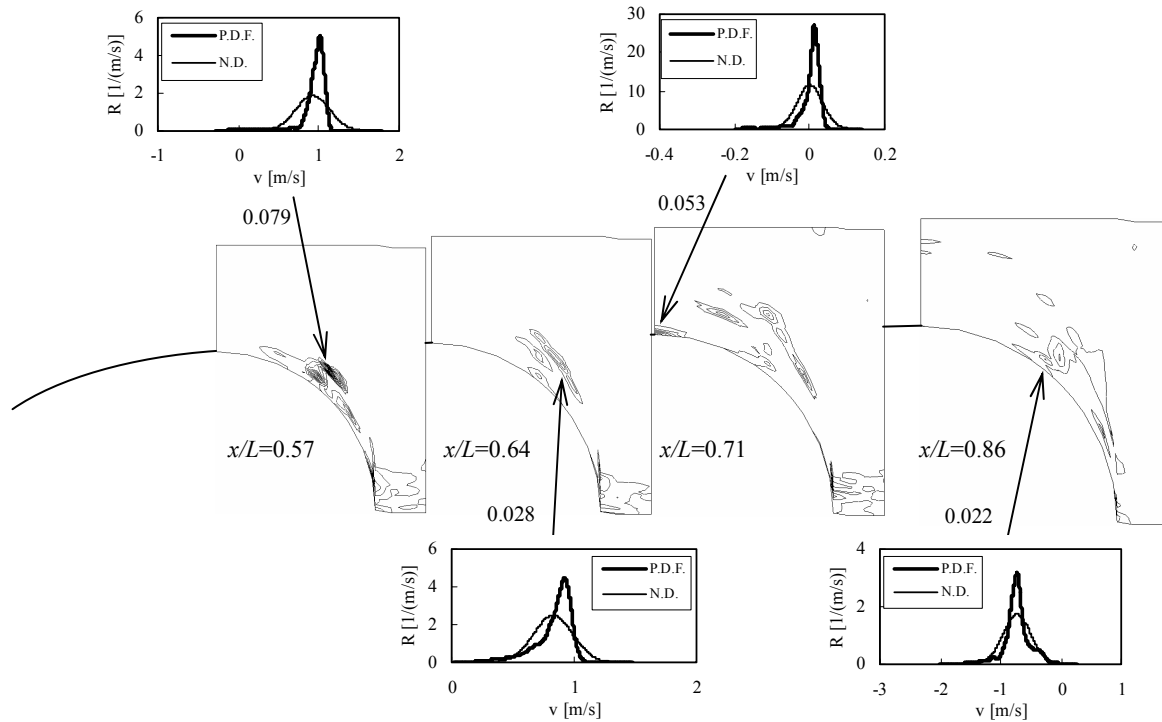
Fig.14 Contour of the product (rms $\times$ Dfn) in each cross section (α=40° , Re=1.8$\times$10^4)

sheet and fog machine at x/L=1.0 in α=50° , Re= 9.0 $\times$ 10^3. In these pictures, it is confirmed that the primary vortex is absorbed to the main vortex, consequently the small vortices generate near the main vortex core. Although such visualization picture is not obtained at x/L=0.43, it is considered that the r.m.s. values of velocity fluctuation and Reynolds stress become large by the same mechanism as x/L=1.0.

5 Conclusions

In this study, we have investigated the separated vortices over axisymmetric paraboloid at high angles of attack. Fluctuation velocity distribution have been measured in detail using hot wire anemometer which has X-type probe. The following conclusions were derived from the results and discussion.

(1)The r.m.s. distribution of velocity fluctuation at 40 and 50 deg angle of attack was measured in detail , so that it was confirmed that the vortex region where the r.m.s. value has a maximum , varied for angle of attack. The

phenomena of the lift-off of longitudinal vortices and the vortex mergence were demonstrated quantitatively. Further, the change of the size for the vortex region could be recognizable by the consistency of the contour in the r.m.s. distribution.

(2)It has been possible to account for quantitatively the kink of vortex cores of primary and secondary vortices at α=40° as a result of assessing the velocity data in the longitudinal vortices using the probability density function and the r.m.s. value of velocity fluctuation. The turbulent separated vortex region have extended to the nose region at α=50° .

(3) The Reynolds stress distribution of velocity fluctuation in each of angles of attack and Reynolds numbers was calculated in four cross sections over the whole of the body , so that it was found that the Reynolds stress value fluctuated in the cross section where the vortex cores of primary and secondary vortices were kinky. The Reynolds stress distribution have become complicated configuration in the backward of the body at α=50° . As a result, it
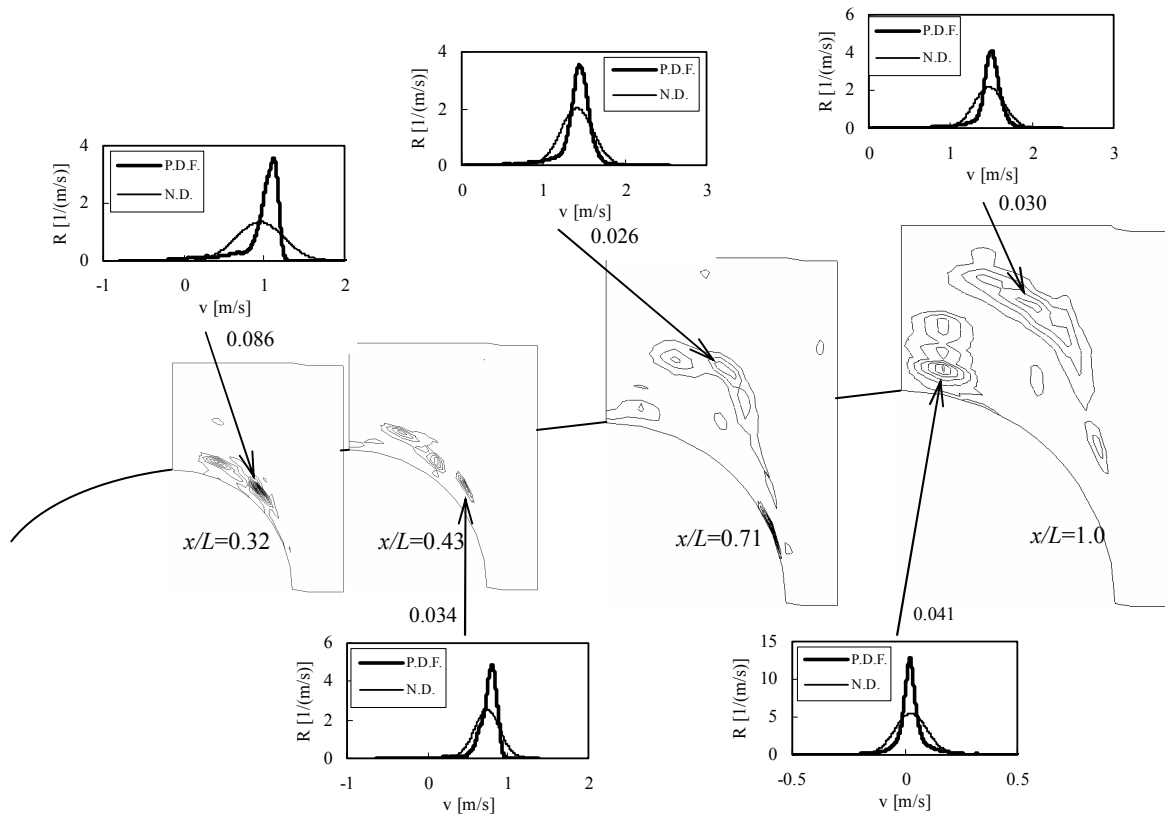
Fig.15 Contour of the product (rms×Dfn) in each cross section (α =50° , Re= 1.8×10^4)

has been estimated that primary vortex has been absorbed into main vortex, and the core of main vortex has fluctuated. Finally, asymmetrical separated vortices have been induced.

References

[1] Jia,M., Watanuki,T. and Kubota,H. : The Visualization of Separated Flow over Slender Bodies at High Angles of Attack, *J.Visualization Soc. Jpn.*, Vol.14,No.55,pp 243-252, 1994.

[2] Poll,D.I.A : On the effects of boundary-layer transition on a cylindrical afterbody at incidence in low-speed flow, *Aeronaut. J.,* pp 315-327,1985.

[3] Barberis,D. and Molton,P. : Experimental Study of Three-Dimensional Separation on a Large-Scale Model, *AIAA J.*, Vol.33,No.11, pp 2107-2113,1995.

[4] Wang,K.C.,Zhou,H.C. and Hu,C.H. : Three-dimensional separated flow structure over prolate spheroids, *Proc.R.Soc.Lond.A*, Vol.421,pp 73-90, 1990.

[5] Meier,H.U. and Kreplin,H.P. : Experimental Investigation of the Boundary Layer Transition and Separation on a Body of Revolution , *Z.Flugwiss. Weltraumforsch.*,4,pp 65-71,1980.
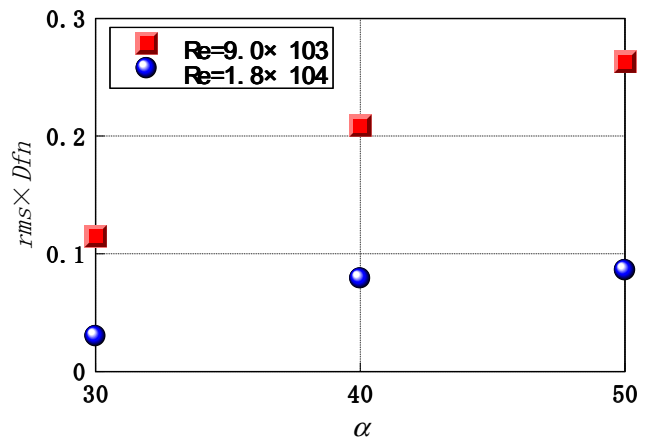
Fig.16 Behavior of the product (rms×Dfn) maximum value

[6] Kreplin,H.P. and Stager,R. : Measurements of the Reynolds-Stress Tensor in the Three-Dimensional Boundary Layer of an Inclined Body of Revolution , *Proc. 9th Symp. "TURBULENT SHEAR FLOWS"* , Kyoto, Japan,pp 2.4.1-2.4.6, 1993.

[7] Chesnakas,C.J. and Simpson,R.L. : Measurements of the Turbulence Structure in the Vicinity of a 3-D Separation, *Trans.ASME*,Vol.118, pp 268-275,1996.

[8] Przirembel,C.E.G. and Shereda,D.E.:Aerodynamics of Slender Bodies at High Angles of Attack, *J. Spacecraft*, Vol.16,No.1,pp 10-14, 1979.

Table.1 Maximum values of the quantity of lifting off the body surface in each separated vortex

Re	Longitudinal vortices	$\alpha=30°$	$\alpha=40°$
9.0×10^3	Main vortex	0.155	0.238
	Primary vortex	0.1	0.104
	Secondary vortex	0.054	0.058
1.8×10^4	Main vortex	0.139	0.229
	Primary vortex	0.083	0.081
	Secondary vortex	0.044	0.041
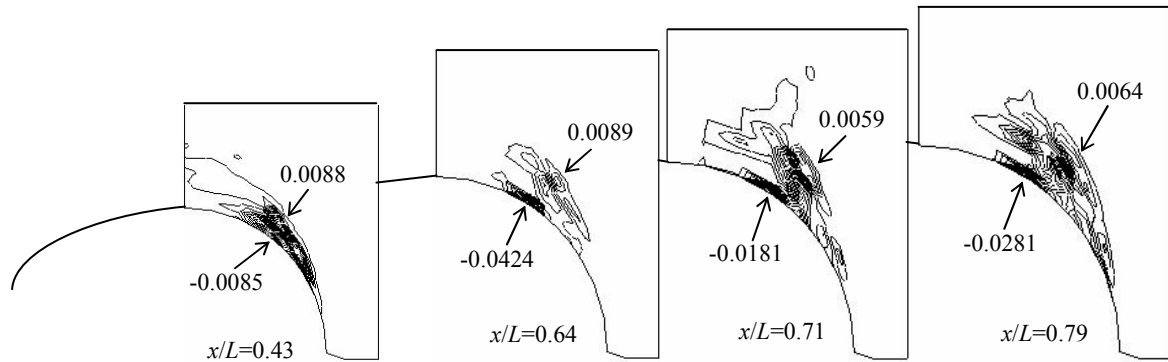
Fig.17 Contour of Reynolds stress (*u'v'*) in each cross section ($\alpha=40°$, *Re*= 9.0×10^3)
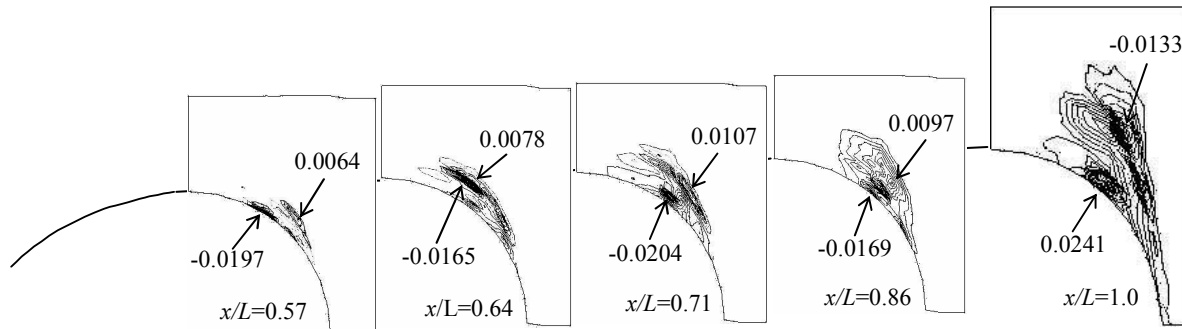
Fig.18 Contour of Reynolds stress (*u'v'*) in each cross section ($\alpha=40°$, *Re*= 1.8×10^4)

[9] Ericsson,L.E. and Reding,J.P.:Dynamics of Forebody Flow Separation and Associated Vortices, *J. Aircraft,* Vol.22,No.4,pp 329-335,1985.

[10] Wardlaw,A.B., Jr. and Yanta,W.J. : Asymmetric Flowfield Development on a Slender Body at High Incidence, *AIAA J.*, Vol.22,No.2,pp 242-249,1984.

[11] Degani,D. and Zilliac,G.G. : Experimental Study of Nonsteady Asymmetric Flow around an Ogive-Cylinder at Incidence, *AIAA J.*, Vol.28,No.4, pp 642-649,1990.

[12] Ishide,T. and Nishikawa,N. : Experimental Study of Unsteady Flow behavior in Separated Flow along

Blunt Body , *Proc. 31st Aircraft Symp.*,pp 140-143,1993.

[13] Nishikawa,N. and Ishide,T. : Visualization and Measurement of Separated Flow over Axisymmetric Paraboloid, *Proc. 2nd Asian-Pacific Conference on Aerospace Technology and Science*, Dun Huang, pp 137-142,1997.

[14] Ishide,T.,Nishikawa,N. and Mikami,F. : Smoke Visualization and Hot Wire Measurements of Three Dimensional Separated Flows, *J. Jpn Soc. Aeronaut. Space Sci.*, Vol.48, No.553,pp 27-33,2000.

[15] Ishide,T.,Nishikawa,N. and Mikami,F.: Experimental Investigation of Three Dimensional Separated Flow
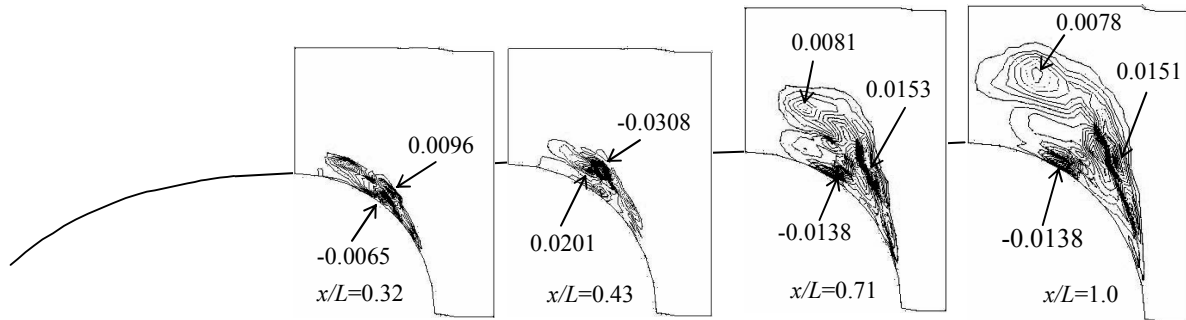
Fig.19 Contour of Reynolds stress ($u'v'$) in each cross section (α=50°, Re= 1.8×10^4)
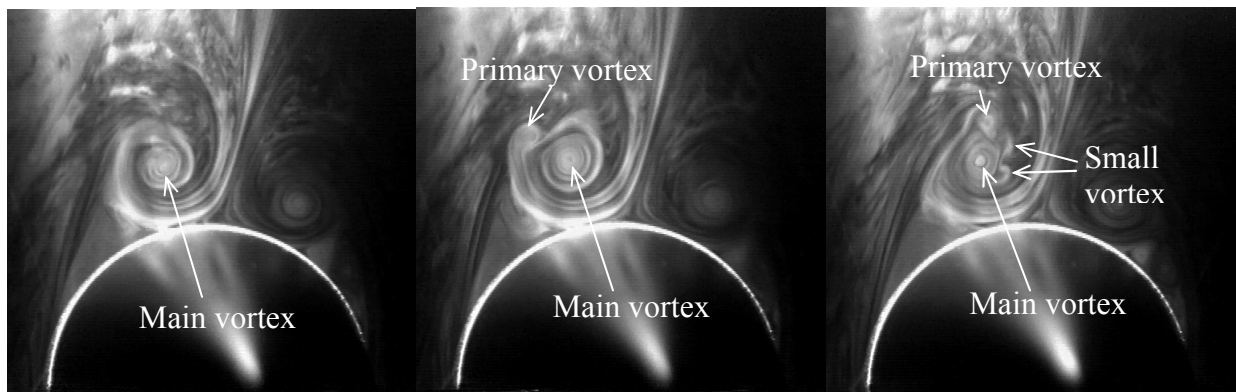
Fig.20 Visualization pictures of the separated vortices (α=40°, Re= 9.0×10^3, x/L=1.0)

over a Body of Revolution at High Angles of Attack ,
CD-ROM Proc. 22nd Int. Congress Aeronaut. Sci.
,U.K., 293.1-293.9,2000